



Andreev Reflection Spectroscopy on SnAs Single Crystals

Sandeep Howlader¹ · Nikhlesh Singh Mehta¹ · M. M. Sharma^{2,3} · V. P. S. Awana^{2,3} · Goutam Sheet¹

Received: 15 January 2022 / Accepted: 19 April 2022 / Published online: 29 April 2022

© The Author(s), under exclusive licence to Springer Science+Business Media, LLC, part of Springer Nature 2022

Abstract

Binary compounds of SnT family (T = As, Sb, Te, S, Se, P) exhibit novel properties like superconductivity and topologically protected states. Some of these compounds crystallize in NaCl type structure or in layered structure, both of which are considered potentially important for high temperature/unconventional superconductivity. It was previously shown that K-doped BaBiO₃ with NaCl type structure exhibits superconducting state below ~30 K. SnAs has crystallographic configuration that is exactly similar to K-doped BaBiO₃ and this warrants for the investigation of superconductivity in this material. Previously it was reported that SnAs exhibits weakly coupled type I superconductivity with an energy gap of 0.7 meV. Recently, the electronic band-structure calculations have hinted to the existence of possible topologically protected states in SnAs. This has motivated us to investigate the superconducting nature of SnAs using point contact Andreev reflection spectroscopy. Our investigation revealed that superconductivity in SnAs can be well-explained within the BCS framework in the weak coupling limit.

Keywords Andreev reflection · Scanning tunneling spectroscopy · Superconductivity

1 Introduction

Recently, investigation of the electronic properties of binary compounds of SnT family (T = As, Sb, Te, S, Se, P) has garnered a lot of attention [1–4]. These materials exhibit novel properties and are considered as sister compounds of topological materials (e.g., topological semimetals and topological crystalline insulators), while some were also found to be superconductors [5]. The SnT family of compounds are also candidate materials for topological superconductivity. In the context of superconductivity, In doped SnTe was found to host an unusual pairing mechanism [6–8]. Among the members of this family of materials, being host to anisotropic

properties, the materials with NaCl-type structure are most widely studied [9–13]. Even though the NaCl-type structural compounds are not layered, due to highly symmetric nature of NaCl-type SnT, it is possible that due to the presence of a single crystallographically independent site for Sn, the typical mixed valence state of Sn (Sn⁴⁺ + (5s⁰) and Sn²⁺ + (5s²)) becomes naturally forbidden. This is quite similar to the case of BaBiO₃ where upon doping with Potassium a high temperature superconducting phase was obtained [14, 15]. Therefore, it becomes highly probable that NaCl-type SnT materials may exhibit high T_c superconductivity.

Tin arsenide (SnAs) is a material that belongs to the SnT family and crystallizes in the NaCl-type structure. SnAs was first demonstrated to exhibit superconductivity by Geller and Hull in 1964 [16]. In 2014, Wang et al. performed transport and heat capacity measurements in SnAs and reported that SnAs exhibits weakly coupled type-I superconductivity ($\lambda = 0.62$) with a low transition temperature of 3.58 K [17]. Additionally, instead of being in a mixed valence state, Sn was found to exist in a single valence state. Phonon dispersion curves and phonon DOS were studied theoretically which revealed that the As p-states hybridize strongly with Sn p-states at the Fermi level [18]. Moreover, DFT calculations revealed that spin–orbit coupling does not have any significant effect on the band structure. However, ARPES

✉ V. P. S. Awana
awana@nplindia.org

Goutam Sheet
goutam@iisermohali.ac.in

¹ Department of Physical Sciences, Indian Institute of Science Education and Research Mohali, S.A.S. Nagar, 81, Knowledge city, Manauli 140306 Punjab, India

² Academy of Scientific & Innovative Research (AcSIR), Ghaziabad 201002, India

³ CSIR, National Physical Laboratory, New Delhi 110012, India

measurements revealed significant band splitting [5]. More recent investigation of electronic band structure and Density of States (DOS) within the Density Functional Theory (DFT) posited the possibility of non-trivial topology in SnAs bands. Furthermore, the band dispersion obtained for SnAs were also found to closely resemble to that of SnTe, a topological crystalline insulator [5]. These calculations also revealed band inversion, gapped states near the Fermi level, and possible existence of topological surface states. This makes SnAs a good system for studying possible topological superconductivity. While the existence of topological surface states is suggested by bandstructure calculations, the nature of superconductivity in SnAs remains an open problem and needs to be investigated using an intimate spectroscopic technique. Observation of unconventional behavior of superconductivity in SnAs would support the possibility of topological superconductivity. In this paper, we investigated the possibility of unconventional superconductivity in SnAs by performing point contact Andreev reflection (PCAR) spectroscopy at low temperatures and under the presence of high magnetic fields.

2 Experimental

The SnAs single crystals used in this study were grown by following a two-step method as described in our previous report [19]. The point contacts Andreev reflection spectroscopy measurements were performed in a liquid helium cryostat which is equipped with a variable temperature insert (VTI) operational between 1.4 and 300 K. The cryostat is also equipped with a superconducting vector magnet (6 T-1 T-1 T). A home-built probe which utilizes the needle anvil method was used to form point contacts at low temperatures. Here, a mesoscopic point contact junction was formed by engaging a silver (Ag) tip on the surface of SnAs single crystal. Contacts where the diameters were small yielded two peaks in dI/dV spectrum, symmetric about the zero bias. These peaks are signature of Andreev reflection phenomenon [20–23]. Andreev reflection process is observed in ballistic point contacts between a normal metal and a superconductor that leads to a special type of non-linearity in the I-V spectrum. For such point contacts, the non-linearity is directly probed in a dI/dV spectrum. Differential conductance spectra obtained in PCAR experiments are analyzed via the Blonder, Tinkham, and Klapwijk (BTK) model [24–28]. Here, the normal metal/superconductor (N/S) interface is modeled as a δ -function potential barrier and its strength is characterized by Z , a dimensionless parameter. For elemental superconductors, the quasi-particle life-time, introduced in the BTK formalism through the broadening parameter Γ , is very small. Differential conductance spectra obtained for mesoscopic interfaces for such superconductors can be fitted

by using just two fitting parameters, the barrier potential and the superconducting energy gap (Δ). For nonzero barrier potential ($Z > 1/4$), the differential conductance spectrum obtained for a ballistic contact contains Andreev peaks at bias $V = \pm \Delta/e$.

3 Result and Discussion

Phase purity of the synthesized SnAs crystal was determined through Rietveld refined XRD pattern, and the result is shown in Fig. 1. The synthesized SnAs crystal has NaCl type cubic structure with Fm-3 m space group symmetry. Parameters obtained from Rietveld refinement are listed in Table 1. More structural details are discussed in our previous report [19]. Superconducting transition near 4 K is evident from inset of Fig. 1 showing field cooled (FC) and Zero field cooled (ZFC) measurements. Magnetization vs. applied Field (M-H) plot at 2 K is shown in left inset of Fig. 1. The wide-open M-H loop shows that the observed superconductivity in synthesized sample gives a hint of weak type-II superconductivity. This result is in contrast with previous reports on SnAs, suggesting the SnAs to be a type I superconductor with a critical field of 150 Oe [5, 17]. More details of the magnetization measurements and the discussion about type I/II superconductivity for SnAs are discussed in detail in ref. 19.

In Fig. 2a, we show a typical point-contact formed using the needle-anvil method. Here, a silver tip was slowly brought into contact with SnAs sample using a differential screw arrangement. The axis of tip coincides with the c-axis of the SnAs crystal with dimensions 4 mm \times 3 mm \times 0.5 mm. After a contact was established, spectroscopic investigation

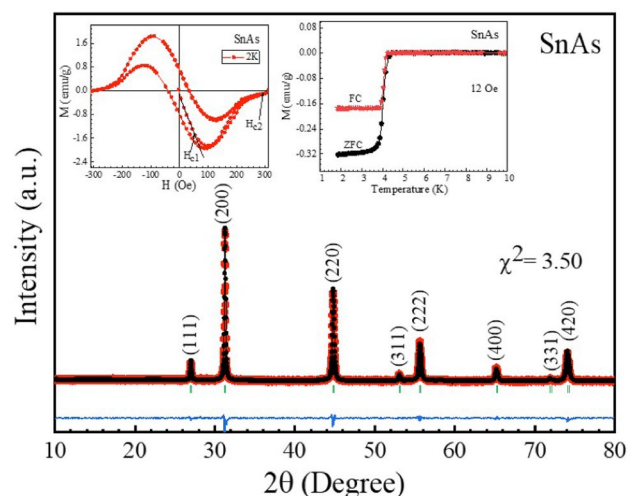


Fig. 1 Rietveld refined XRD pattern of synthesized SnAs crystal, right inset is showing FC and ZFC measurements of SnAs, and left inset is showing M-H plot at 2 K of synthesized SnAs crystal [21]

Table 1 Rietveld refined lattice parameters of SnAs

Sample	a (Å)	b (Å)	c (Å)	α	β	γ
SnAs	5.721(9)	5.721(9)	5.721(9)	90°	90°	90°

was performed. The corresponding normalized dI/dV spectrum obtained for the contact is shown in Fig. 2b where the spectrum was normalized to the conductance at the highest bias value. The spectrum was fitted under the BTK formalism and corresponding fitting parameters used are shown in the figure. It is clearly seen that the spectrum is well-fitted in the range ± 2 mV. Additionally, the spectrum also contains two dips in dI/dV at a higher bias arising due to critical current dominated non-linearities in I-V. Differential conductance spectra obtained for a purely ballistic contact can be

fitted in the entire range under the BTK formalism. However, additional features due to non-linearities in I-V that arise due to factors related to scattering mechanisms occurring within the contact cannot be fitted within the BTK theory and leads to under-estimation of superconducting energy gap (Δ). By fitting the dI/dV spectra, we estimate Δ to be ~ 0.62 meV. This is in agreement with the specific heat results obtained by Bezotosnyi et al. [5].

In order to gain further understanding of the superconducting phase, detailed field and temperature dependent

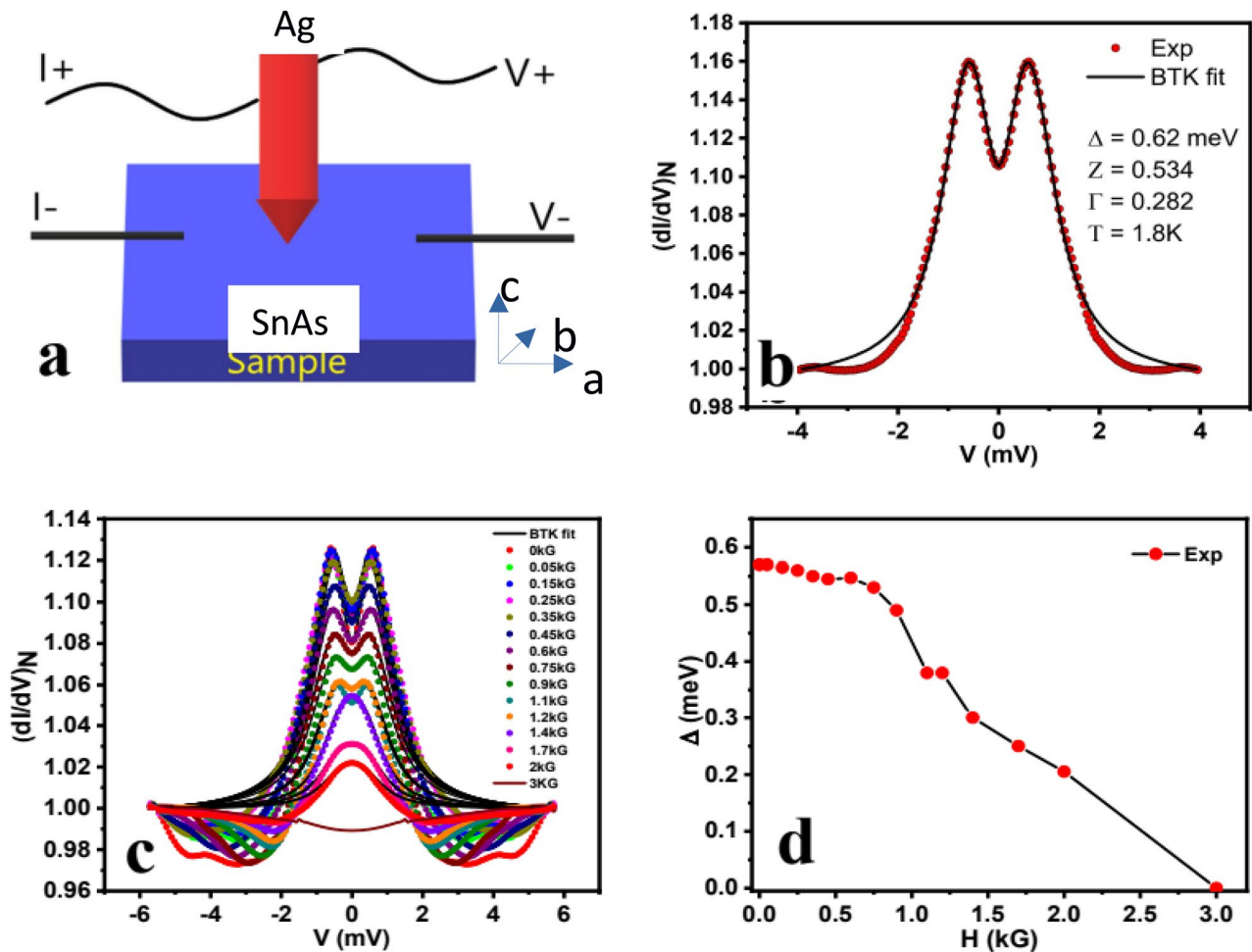


Fig. 2 a Needle-anvil technique of point contact formation depicting the SnAs sample geometry and Silver (Ag) tip in contact, b a differential conductance (dI/dV) spectrum obtained in the ballistic regime with corresponding BTK simulated curve along with the values of simulation parameters, and c Field dependence of dI/dV spectrum along with BTK-simulated curves with magnetic field applied along the Z direction (c-axis) of the crystal. The field dependence was per-

formed at $T = 1.96$ K. The experimental data was normalized and smoothed and presented as dots. The black lines represent the BTK simulated curves. The dI/dV spectrum evolved smoothly with applied field and all spectral features disappeared above 3 kG (d) Δ vs. H plot showing that the superconducting energy gap evolved smoothly with applied magnetic field. The variation of parameters Z, Γ with magnetic field is presented in the Supplemental File

measurements were carried out. We applied magnetic field along the axis of the point contact (B||c). The dI/dV spectra evolved smoothly with applied magnetic field (shown in Fig. 2c). The critical field for a superconducting point contact is the applied field strength for which the peak-dip structure completely vanishes. For our case this happened at 3 kG. All of the spectra were fitted according to the BTK formalism and information regarding change of energy gap with field was extracted. Additionally, with increasing magnetic field, the critical current dip structure was observed to shift inwards. We present the change in Δ with applied magnetic field in Fig. 2d, where the energy gap is seen to decrease monotonically with applied field strength.

We also studied field dependent measurements on some of the other point contacts, where critical current dominated

effects were prominent (shown in Fig. 3). Critical current here refers to the current at which superconductivity is destroyed and the material behaves as a normal metal. The critical current dominated effects appear as dips in the differential conductance spectrum. These dips usually appear at voltage bias between the Andreev peaks and normal state conductance [21]. Recent theoretical simulations on non-ballistic transport in N/S interface revealed that formation multiple point contacts could result in observation of unusual spectroscopic features in PCAR spectrum [32]. However, in case of tunneling spectroscopy (NIS), there are several possible mechanisms behind emergence of such dips such as inelastic tunneling, electron density of states, and band structure change. Such dip-hump structure is known to appear in tunneling spectra of cuprate superconductors [33–36].

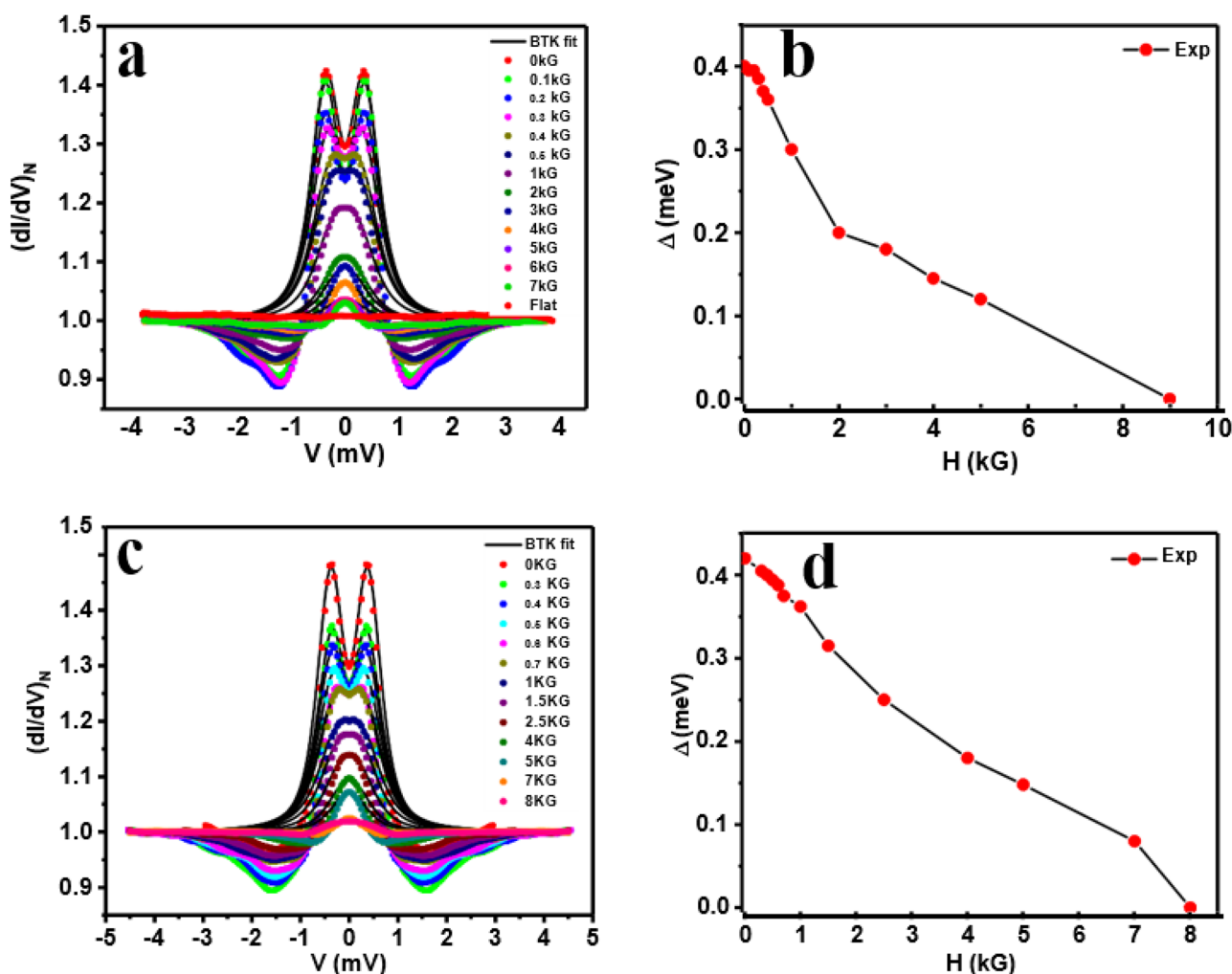


Fig. 3 **a, c** Magnetic field dependence of point contact spectra along with BTK-simulated curves performed at $T=2.06$ K and $T=1.8$ K, respectively, with field applied along the c -axis of the crystal. The experimental data was normalized and smoothed and presented as dots. The black lines represent the BTK simulated curves. The con-

ductance spectrum evolved monotonically with applied magnetic field and all spectral features disappeared above 8 kG. **b, d** corresponding Δ vs. H plot showing that the superconducting energy gap evolved smoothly with applied magnetic field. The variation of parameters Z , Γ with magnetic field is presented in the Supplemental File

These measurements are shown in Fig. 3. Both spectra were seen to evolve monotonically with applied magnetic field. These spectra were also fitted according to the BTK theory and were normalized to the conductance at highest bias value. The estimated value of Δ for these contacts is lower than the estimated value for spectra presented in Fig. 2b. This reduction is a result of analyzing a spectrum where critical current dominated features are present. As we have mentioned before, such features lead to underestimation of energy gap. The overall spectroscopic features for these point contacts vanished at a critical field of 8 kG.

The critical field obtained for spectra shown in Fig. 3 is higher than the spectra shown in Fig. 2c. Before explaining this difference in critical field, let us first iterate that while the modified BTK theory that includes the broadening parameter Γ can describe the dI/dV spectrum in presence of magnetic field [31], it cannot be used to differentiate

between a type-I and type-II superconductor. For a type-I superconductor, in the confined geometry of a point contact, the presence of non-superconducting tip might lead to enhanced local disorder. Such local enhancement in disorder leads to a reduction in the local mean free path and consequently a reduction in local coherence length of the superconducting fraction in the point contact. This effectively drives the superconductor towards type-II regime i.e., the Ginzburg-Landau parameter becomes larger than $1/\sqrt{2}$. This was earlier observed in Pb, which under confinement to mesoscopic dimensions loses its type-I behavior [38–41]. The point contacts may exhibit different critical fields facilitated by such local disorders and impurities which is precisely observed here. Furthermore, either the confined geometry, enhanced local disorder, or both can lead to a difference between the bulk critical field and critical field under a point contact [42].

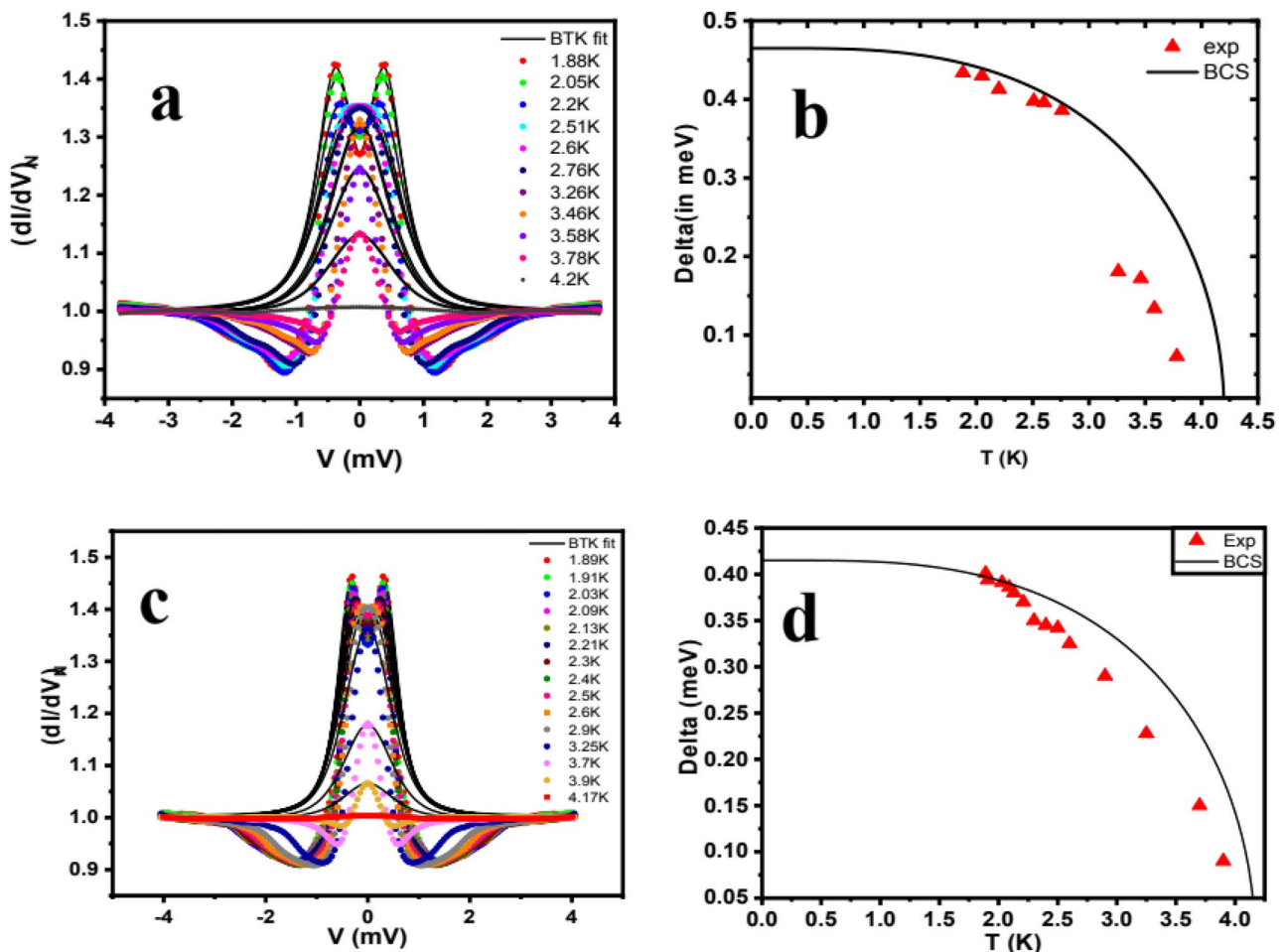


Fig. 4 a, c Temperature dependent evolution of differential conductance spectra obtained for SnAs/Ag point contact ($B=0$ Oe). The experimental data was normalized and smoothed and presented as dots. The black lines represent the BTK simulated curves. Spectral features such as the Andreev peaks and critical current dips dimin-

ish monotonically with increasing temperature and these features completely disappear around 4.2 K. b, d corresponding Δ vs. T with BCS fitting curve. The variation of parameters Z , Γ with temperature is presented in the Supplemental File [37]

We present the temperature dependent measurements in Fig. 4. Here, we show temperature dependent data for point contacts where both, spectroscopic signatures associated with Andreev reflection and critical current of point contact, are present. The data is normalized to the conductance at the highest bias value. As expected for superconductors, the spectra evolved smoothly with increasing temperature and the overall spectroscopic features disappeared above 3.8 K. The flat line in the Fig. 4a, c represents dI/dV spectrum obtained at 4.2 K. Again, as in the case of field dependence, the spectroscopic features appearing due to critical current (dips in dI/dV vs. V) shift towards lower bias value. This indicates temperature dependent suppression of critical current for the point contacts.

Superconducting energy gap and its variation with temperature was obtained by fitting the data under the BTK framework. We have shown the temperature variation of Δ in Fig. 4b, d. The dots represent the estimated value of Δ from BTK simulation of experimental data and the solid line represents the simulated curve following the BCS prediction [29, 30]. The corresponding variation in Z and Γ with temperature is presented in Supplemental File [37]. For Fig. 4b, a sharp decrease in Δ and Z is observed which indicates towards a possible mechanical instability in the point contact. Furthermore, such behavior may also result as fault in fitting. However, error in determining Δ increases with temperature and the values obtained in the range 1.8–2.8 K have least error in estimation. The obtained variation of Δ with temperature aligns with the BCS prediction. Furthermore, the value of Δ as determined by BTK simulation provides the ratio $\Delta(0)/k_B T_c$ within the range 1.2–1.78 indicating that superconductivity in SnAs can be explained by BCS theory in the weak coupling limit. Additionally, we did not detect any features associated with unconventional nature of superconductivity.

4 Conclusion

In conclusion, we performed spectroscopic investigation of superconductivity in NaCl structure crystallized SnAs single crystals and obtained a superconducting energy gap of 0.62 meV, estimated from a ballistic point contact. On the basis of detailed temperature and field dependence of various point contacts on SnAs, and corresponding BTK simulated curves, and BCS ratio, it can be said that superconductivity in SnAs can be explained within the BCS framework. The critical temperature for the superconducting point contacts was found to be around 4.2 K with a critical field in range 3–8 kG. On the basis of detailed PCAR spectroscopic investigation, it may be inferred that SnAs behaves as a conventional superconductor.

Supplementary Information The online version contains supplementary material available at <https://doi.org/10.1007/s10948-022-06261-1>.

Funding The study received financial support from the University Grants Commission, India, and from the Swarnajayanti fellowship awarded by the Department of Science and Technology (DST), Govt. of India (grant No. DST/SJF/PSA-01/2015–16).

References

- Zhao, L.-D., Lo, S.-H., Zhang, Y., Sun, H., Tan, G., Uher, C., Wolverton, C., Dravid, V.P., Kanatzidis, M.G.: *Nature* **508**, 373 (2014)
- Sun, Y., Zhong, Z., Shirakawa, T., Franchini, C., Li, D., Li, Y., Yunoki, S., Chen, X.-Q.: *Phys. Rev. B* **88**, 235122 (2013)
- Kamitani, M., Bahramy, M.S., Nakajima, T., Terakura, C., Hashizume, D., Arima, T., Tokura, Y.: *Phys. Rev. Lett.* **119**, 207001 (2017)
- Hsieh, T.H., Lin, H., Liu, J., Duan, W., Bansil, A., Fu, L.: *Nat. Commun.* **3**, 982 (2012)
- Bezotosnyi, P.I., Dmitrieva, K.A., Sadakov, A.V., Pervakov, K.S., Muratov, A.V., Usoltsev, A.S., Tsvetkov, A.Yu., Gavrilkin, S.Yu., Pavlov, N.S., Slobodchikov, A.A., Vilkov, O.Yu., Rybkin, A.G., Nekrasov, I.A., Pudalov, V.M.: *Phys. Rev. B* **100**, 184514 (2019)
- Erickson, A.S., Chu, J.H., Toney, M.F., Geballe, T.H., Fisher, I.R.: *Phys. Rev. B* **79**, 024520 (2009)
- Balakrishnan, G., Bawden, L., Cavendish, S., Lees, M.R.: *Phys. Rev. B* **87**, 140502 (2013)
- Novak, M., Sasaki, S., Kriener, M., Segawa, K., Ando, Y.: *Phys. Rev. B* **88**, 140502 (2013)
- Hullinger, F., Hull, G.W.: *Solid state commun.* **8**, 1379 (1970)
- Tutuncu, H.M., Bagci, S., Srivastava, G.P., Akbulut, A.: *J. Phys.: Condens. Matter* **24**, 455704 (2014)
- Wang, Z., Wang, J., Zang, Y., Zhang, Q., Shi, J.-A., Jiang, T., Gong, Y., Song, C.-L., Ji, S.-H., Wang, L.-L., Gu, L., He, K., Duan, W., Ma, X., Chen, X., Xue, Q.-K.: *Adv. Mater.* **27**, 41506 (2015)
- Tanaka, Y., Ren, Z., Sato, T., Nakayama, K., Souma, S., Takahashi, T., Segawa, K., Ando, Y.: *Nat. Phys.* **8**, 800 (2012)
- Tanaka, Y., Shoman, T., Nakayama, K., Souma, S., Sato, T., Takahashi, T., Novak, M., Segawa, K., Ando, Y.: *Phys. Rev. B* **88**, 235126 (2013)
- Cava, R.J., Batlogg, B., Krajewski, J.J., Farrow, R., Rupp, L.W., Jr., White, A.E., Short, K., Peck, W.F., Kometani, T.: *Nature* **332**, 814 (1988)
- Mattheiss, L.F., Gyorgy, E.M., Johnson, D.W., Jr.: *Phys. Rev. B* **37**, 3745 (1988)
- Geller, S., Hull, G.W.: *Phys. Rev. Lett.* **13**, 127 (1964)
- Wang, Y., Sato, H., Toda, Y., Ueda, S., Hiramatsu, H., Hosono, H.: *Chem. Mater.* **26**(24), 7209 (2014)
- Tutuncu, H.M., Srivastava, G.P.: *Solid State Commun.* **221**, 24 (2015)
- Sharma, M.M., Sharma, P., Gurjar, G., Patnaik, S., Awana, V.P.S.: *Solid state Commun.* **340**, 114531 (2021)
- Duif, A.M., Jansen, A.G.M., Wyder, P.: *J. Phys. Condens. Matter* **1**(20), 3157 (1989)
- Sheet, G., Mukhopadhyay, S., Raychaudhuri, P.: *Phys. Rev. B* **69**, 134507 (2004)
- Jansen, A.G.M., Van Gelder, A.P., Wyder, P.: *J. Phys. C Solid State Phys.* **13**(33), 6073 (1980)
- Yanson, I.K.: *Sov. Phys. JETP* **39**, 506 (1974)
- Andreev, A.F.: *JETP* **46**, 1823 (1964)
- Daghero, D., Gonnelli, R.S.: *Supercond. Sci. Technol.* **23**, 043001 (2010)
- Klapwijk, T.M., Ryabchun, S.A.: *J. Exp. Theor. Phys.* **119**, 997 (2014)

27. Blonder, G.E., Tinkham, M.M., Klapwijk, K.T.: *Phys. Rev. B* **25**, 7 (1981)
28. Strijkers, G.J., Ji, Y., Yang, F.Y., Chien, C.L.: *Phys. Rev. B* **63**, 104510 (2001)
29. Gasperovic, R.F., Taylor, B.N., Eck, R.E.: *Solid state communication* **4**, 59 (1966)
30. Bardeen, J., Cooper, L.N., Schrieffer, J.R.: *Phys. Rev.* **108**, 1157 (1957)
31. Naidyuk, Yu.G., Gloos, K.: *Low Temp. Phys.* **44**, 257 (2018)
32. Kumar, R., Sheet, G.: *Phys. Rev. B* **104**, 094525 (2021)
33. Chi, S., Aluru, R., Grothe, S., Kreisel, A., Singh, U.R., Andersen, B.M., Hardy, W.M., Liang, R., Bonn, D.A., Burke, S.A., Wahl, P.: *Nat. Comm.* **8**, 15996 (2017)
34. Allan, M.P., Lee, K., Rost, A.W., Fischer, M.H., Masee, F., Kihou, K., Lee, C.H., Iyo, A., Eisaki, H., Chuang, T.M., Davis, J.C.: *Nat. Phys.* **11**, 177–182 (2015)
35. Ponomarev, Y.G., Van, H.H., Kuzmichev, S.A., Kulbachinskii, S.V., Mikheev, M.G., Sudakova, M.V., Tchesnokov, S.N.: *JETP Lett.* **96**, 743–749 (2013)
36. Gabovich, A.M., Voitenko, A.I., Ekino, T., Li, M.S., Szymczak, H., Pekała, M.: *Adv. Condens. Matter Phys.* **2010**, 681070 (2010)
37. See supplemental material file. <https://doi.org/10.1007/s10948-022-06261-1>
38. Yang, C., Tsao, F., Wu, S., Li, W.-H., Lee, K.: *J. Low Temp. Phys.* **131**, 349 (2003)
39. He, M., Wong, C.H., Tse, P.L., Zheng, Y., Zhang, H., Lam, F.L., Sheng, P., Hu, X., Lortz, R.: *ACS Nano* **7**, 4187 (2013)
40. Rodrigo, J.G., Crespo, V., Suderow, H., Vieira, S., Guinea, F.: *Phys. Rev. Lett.* **109**, 237003 (2012)
41. Sirohi, A., Saha, P., Gayen, S., Singh, A., Sheet, G.: *Nanotechnology* **27**, 285701 (2016)
42. Datta, S., Howlader, S., Singh, R.P., Sheet, G.: *Phys. Rev. B* **105**, 094504 (2022)

Publisher's Note Springer Nature remains neutral with regard to jurisdictional claims in published maps and institutional affiliations.